A system for the study of magnetic materials and magnetic imaging with the scanning tunneling microscope

P. N. First, Joseph A. Stroscio, D. T. Pierce, R. A. Dragoset, and R. J. Celotta
National Institute of Standards and Technology, Gaithersburg, Maryland 20899

(Received 24 July 1990; accepted 28 November 1990)

A report of work in progress to determine the feasibility of imaging the magnetization of ferromagnetic samples with the scanning tunneling microscope (STM) is presented. A vacuum system was designed to test several different proposals as well as to prepare and characterize thin films of magnetic materials by conventional means, including STM. This was begun with an attempt to detect spatially resolved spin-polarization of secondary electrons emitted from the sample when operating the STM in the scanning field emission mode. Results are currently inconclusive, but encouraging. A weak spin-polarization signal has been observed corresponding to one of the in-plane components of magnetization. However, topographic feedthrough has not been fully eliminated as a possible spurious source of contrast.

I. INTRODUCTION

Techniques for achieving high resolution magnetic imaging have become more important since the advent of high density magnetic disks for data storage. It is apparent that as the size of magnetic bits decreases, the resolution of diagnostic tools must increase concurrently. Of equal importance, however, is the capability of these techniques to provide fundamental information about magnetic phenomena such as domain formation and magnetism at surfaces. In particular, some of our current interests concern the growth of thin films of magnetic materials. For these systems it is especially important to correlate aspects of the film growth with the resultant magnetization in order to understand the novel and controversial properties associated with these materials.[1] To make this correlation as direct as possible, we have sought to integrate the capabilities of scanning tunneling microscopy with nanometer-scale magnetic imaging of the same microscopic region. Ultimately one would like to attain atomic resolution of the magnetization in order to finely resolve structure within, for example, domain walls, magnetic singularities, and antiferromagnets.

A number of methods for obtaining magnetic contrast with the scanning tunneling microscope (STM) have been proposed (e.g., Refs. 2 and 3), each with associated challenges. Some of the more promising of these methods are (1) tunneling with a spin-polarized tip, e.g., a ferromagnet, antiferromagnet, or optically pumped GaAs; (2) detection of the optical polarization of recombination luminescence from tunneling into a GaAs tip, which depends upon the polarization of tunneling electrons; and (3) detection of the spin-polarization of secondary electrons generated by a scanning field emitter tip. The first two methods are in principle capable of atomic resolution since they operate in the tunneling mode, while the resolution of the latter is dependent upon the quality of the emitter tip. Fink[4,5] has achieved 3 nm resolution in images of the intensity of emitted electrons by preparing very low voltage emitter tips under the field ion microscope. We have designed an apparatus flexible enough to pursue several of these techniques, in addition to standard STM investigations. This paper is a preliminary report of our efforts to determine the viability of the scanning field emission technique for imaging the sample magnetization.

Although it may not achieve true atomic resolution, we chose to begin with scanning field emission for a number of reasons. First, the field emission tip is nonmagnetic, and thus cannot affect the magnetic structure of the sample. This is particularly important for studies of ferromagnetic surfaces. Second, the method is conceptually a simple extension of the scanning electron microscopy with polarization analysis (SEMPA) technique[6] used successfully in several laboratories, including our own, with the best spatial resolution to date near 30 nm. As with SEMPA, the scanning field emission microscopy could, in principle, measure all three components of the vector magnetization. Third, insights gained from this technique should be applicable to other secondary electron microscopies, e.g., scanning Auger. Finally, even if atomic resolution is not attained, the technique should still have the capability to "zoom" from magnetization images, perhaps at 10 nm resolution, to conventional STM topographs at the atomic scale. Quite direct correlations could therefore be made between the film morphology and magnetic properties.

In the following section the technique and apparatus are described in more detail, while in Sec. III we present some preliminary results. A brief summary appears in Sec. IV.

II. EXPERIMENT

It has been established experimentally[6] that the spin-polarization of secondary electrons emitted from a clean ferromagnetic surface reflects the magnetization of that surface. This is the foundation of the SEMPA technique. In SEMPA, both the intensity and polarization of emitted secondary electrons are monitored as the electron microscope beam is rastered across the sample surface. This results in a standard SEM image being measured concurrently with maps of the vector components of the magnetization.

The present experiment is similar to SEMPA, with the electron microscope gun replaced by a scanning field emission tip. Figure 1 illustrates the geometry. A conventional STM is operated in the field emission regime so that elec-

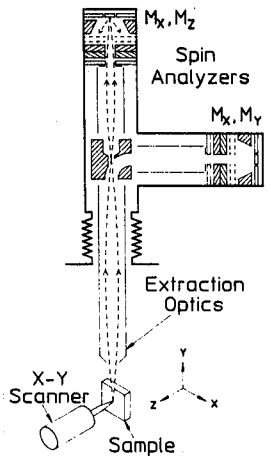

FIG. 1. Schematic of the experimental geometry for collecting electrons ejected by the scanning field emission tip. The extraction optics input is biased at + 1500 V with respect to the sample, but the collected electrons are subsequently retarded by 1350 eV for spin-analysis.

trons incident on the sample have enough energy to generate secondaries. The STM servo is still used to maintain a nominally constant tip–sample separation (as in Young's original topografiner),[7] but a gain increase of at least a factor 10 is generally necessary to accommodate a reduced sensitivity to separation in the field emission mode. Emitted secondary electrons are then collected by the 1500 V extraction optics (at 90° with respect to the sample normal) and, in principle, are directed to either of two electron spin-analyzers, although only the analyzer detecting M_x and M_z components has been mounted for these preliminary measurements. The analyzers are of the backscattering type developed in this group[8,9] and are notable for their small size and high efficiency. All electron optical components are mounted directly above the STM on an XYZ manipulator for fine position control.

The actual experimental apparatus consists of a 250 mm o.d. ultrahigh vacuum chamber (base pressure $\sim 8 \times 10^{-11}$ Torr) with a horizontal cylinder axis. A circle of four 200 m o.d. flanged ports accommodate the ion and sublimation pumps, low-energy electron diffraction/Auger, sample manipulator, and a viewport, while a similar circle at the opposite end of the chamber houses the STM, a field ion microscope (FIM), electron optics, and another viewport. Load-lock, wobble sticks, tip parking, sputter gun, evaporators, and more viewports are incorporated into two 340 mm o.d. flanges on the ends of the chamber. Other side ports are used for a sample carousel, turbo pump, and vacuum gauges. At one end of the chamber, samples can be cleaned and characterized by LEED and Auger before depositing a metal overlayer if desired. Both samples and tips are transferred across the chamber using a pincer-grip wobble stick and a magnetically coupled linear/rotary feedthrough. There the sample is transferred to the STM with another wobble stick, while the tip can be inserted into either the FIM (where all preparation is done) or the STM.

The STM consists of a double piezoelectric tube scanner, similar to that described by Lyding *et al.*,[10] with a 12.5 mm outer tube and 6 mm inner tube, both 16 mm long. The Z axis motion is effected using the outer piezo, while the inner tube generates the X–Y raster. This arrangement minimizes coupling between the Z axis and those in plane, and also allows for the inside electrode of the 6 mm tube to be grounded, thus shielding the tunnel current lead connected to the tip holder. The tunnel current signal is fed directly to a FET preamp (10^8 V/A) mounted on the same vibration stage to reduce the effect of pickup from microphonics and ground loops. A commercially available beryllium copper socket, suitable for 1 mm diam rods, is used as the tip holder. It is mounted on the scanner axis using a ceramic fitting and UHV epoxy. The emitter tips themselves consist of short lengths ($\sim$4 mm) of 0.25 mm diam W(111) oriented wire, spot-welded to 1 mm diam polycrystalline tungsten shanks about 10 mm long. The single crystal wire is electrochemically etched to the desired profile using Melmed's method[11] of etching under an optical microscope. After use in the STM a tip can be reetched a number of times by this technique. A spring clip holds the sample to a molybdenum block, which can be positioned along the X and Z axes using two orthogonal inchworm motors[12] to push or pull the block as required. Play of $\sim$1 mm in this push/pull coupling allows us to decouple the inchworms during the actual measurements, eliminating any resonance associated with these devices. A ground quartz plate provides the sliding surface for three Be–Cu balls on the bottom of the sample block. Vibration isolation is accomplished using a two stage, eddy-current damped spring suspension system with a resonance of $\sim$3 Hz, and the entire assembly is mounted on a 200 mm flange that occupies one of the bottom ports on the system.

The field ion microscope was also designed to fit on a 200 mm flange and mates to a neighboring port. It is comprised of a nominally 12 kV feedthrough (onto which the tip is mounted) welded into a stainless steel reservoir for liquid nitrogen. Two 6 mm o.d., stainless tubes connect the reservoir and a 40 mm diam microchannel plate image intensifier to the 200 mm flange. Liquid nitrogen and high voltage feedthroughs run through miniflange ports in the side of the 200 mm flange, with other electrical and thermocouple feedthroughs coming out similar ports on the back. A rotary motion feedthrough on one of these ports also allows insertion of a heater or mask hole in front of the emitter tip. The 2.5 mm mask hole in a 0.25 mm stainless steel plate at ground potential can be positioned within about 2 mm of the high voltage tip, thus permitting lower image voltages by decreasing the field reduction factor[13] of the microscope from nearly 10 to $\sim$6.5. For field emission imaging the mask is not used, and the actual tip–screen distance is 24 mm. A window is welded directly into the center of the 200 mm flange for viewing the phosphor screen of the image intensifier.

Two important questions must be answered to determine the usefulness of the scanning field emission technique for magnetic imaging: (1) can true secondary electrons be collected in sufficient quantity to analyze their spin, and (2) what spatial resolution can be obtained? Allenspach and Bischof[14] have previously demonstrated that spin-polarized secondary electrons can be obtained using a field emission

tip, though at a distance of ~1 mm from the sample surface, where the spatial resolution is too poor to be useful. A difficulty here is that the voltage applied to obtain field emission from the tip also sets up a field that forces low energy secondaries back into the sample.[2,15] For a given emitter tip, the spatial resolution increases with decreasing tip–sample separation, while the number of secondaries escaping from the region beneath the tip will decrease. To reduce the effect of this field, a low voltage field emitter is desirable, as is a small divergence of the field emitted beam to maintain adequate resolution at larger tip–sample spacings.

Following Fink,[4,5] we have adapted the method of Janssen and Jones[16] to fabricate such emitter tips for use in the scanning field emission mode. However, our aim for this experiment is not to obtain a single atom electron source as Fink has done, since this would result in field emission below 20 V, where the contribution of true secondaries to the total electron yield becomes very small.[17] Consequently we are able to prepare adequate emitter tips at room temperature, which reduces contamination as well as subsequent drift in the STM. The tip is first cleaned by electron bombardment heating to roughly 1500 K, after which the field emission threshold is typically 250–450 V, as judged by the appearance of a pattern in the image intensifier (operated at 1500 V). Field evaporation in $1–5\times10^{-5}$ Torr He is then used to obtain an end form of greater than 20 nm radius, which is subsequently exposed to 10^{-4} Torr Ne for sputtering. The sputtering technique follows Janssen and Jones,[16] with the exception of our using $W(111)$ oriented tips. The tip is held at a negative potential which is continuously decreased in order to maintain a 20 μA sputtering current. The potential provides a rough estimate of tip radius, with acceptable tips generally obtained for sputtering voltages below 300 V. A short anneal (1–2 sec) to roughly 1000 K stabilizes the tip configuration, and subsequently the field emission pattern often consists of a single emission spot with a threshold below 100 V. If these criteria are not met, sputtering and annealing are repeated, as is the entire process occasionally. It is important that the voltage for electron bombardment annealing be kept low enough to prevent field evaporation at the elevated temperature; in practice we use 500 V and 15 mA emission current with our particular heater geometry. Using these methods, tips with field emission thresholds as low as 60 V have been obtained, producing 1 μA emission current below 220 V. Thresholds of 80–100 V are more typical, with 1 μA emission at 300–380 V. Note that the voltage necessary to achieve 10 nA current at ~100 nm spacing in the STM is usually a factor 2–3 less than the field emission thresholds measured using the image intensifier.

III. RESULTS

In order to explore the feasibility of scanning field emission for magnetic measurements, we have chosen a test sample consisting of several arrays of rectangular Permalloy bits, 50 nm thick, deposited on a Si substrate.[18] This provides a sample with magnetic area on a nonmagnetic background so that contrast should be observed even if the magnetic bits are single domain. The sample was cleaned by several cycles of sputtering with 1 keV Ne ions at a current density of ~2 μA/cm^2. Figure 2 shows a STM style topograph of nine bits, each 0.5 μm square, obtained with a tip bias of −32 V, well into the field emission regime. It must be mentioned that none of the images displayed here are corrected for nonlinearities in the piezo displacements. While the image quality of Fig. 2 is marred by numerous tip-related current jumps, it is clear that this mode—the topografiner mode—is quite useful for surveying a large area very quickly. Since the nominal tip–sample separation is very large (100 nm in this case), even sharp features of great vertical extent can be imaged at scan rates of order 1 μm/sec. The large separation at such low emission voltage was attained only after preparing the tip in the manner described previously.

Current jumps appear to be much more numerous for images taken in the field emission regime than for normal tunneling topographs. These could be a consequence of the larger active area of the field emission source relative to the tunneling probe, thus increasing the probability of an adsorbate atom diffusing into the active area and changing the current. Stimulated desorption of ions from the sample surface may also contribute to this problem.

Figure 3 shows profiles of the electron yield obtained by scanning the field emitter across the central magnetic bit of Fig. 2 at various bias voltages. Figure 5(b) shows the full image from which the −38 V profile was taken. The STM servo loop remains closed during the data acquisition to maintain a nominally constant tip–sample separation, thus providing the topographic map concurrent with a map of the collected electron intensity. Good contrast is found in the intensity profiles, with the region over the bit producing 25%–50% fewer electrons than the silicon substrate, as shown by the average minimum and maximum count rates quoted in the figure caption. Note that these rates are measured after elastic backscattering from the gold target of the spin-analyzer and are therefore of order 100 times less than should be expected for direct detection.

The observation of a decrease in electron yield over the Permalloy is contrary to scanning electron microscopy (SEM) images of this sample using secondary electrons.[19] With a 10 keV SEM beam, the secondary yield of the Permalloy bits was found to be greater than that of the silicon substrate. This raises the question of whether we are imaging secondary, backscattered, or multiply scattered electrons from the scanning field emission experiment. The contrast reversal between SEM and the present measurements could be due to a crossover in the relative secondary yield between Si and Permalloy at low energies, but may also be related to the deflection of backscattered and secondary electrons by high electric fields between the tip and the edges of the bit. Atomic number contrast in the backscattered electrons is expected to result in a greater number of electrons from the Permalloy than from the silicon, contrary to the observations. In any case, quasielastic backscattered electrons should be largely absent for the −45 V profile, because our electron optics admit only those electrons leaving the sample with less than ~40 eV kinetic energy. Since this profile actually shows the greatest contrast, we conclude that a significant portion of the collected electrons are true secondaries or

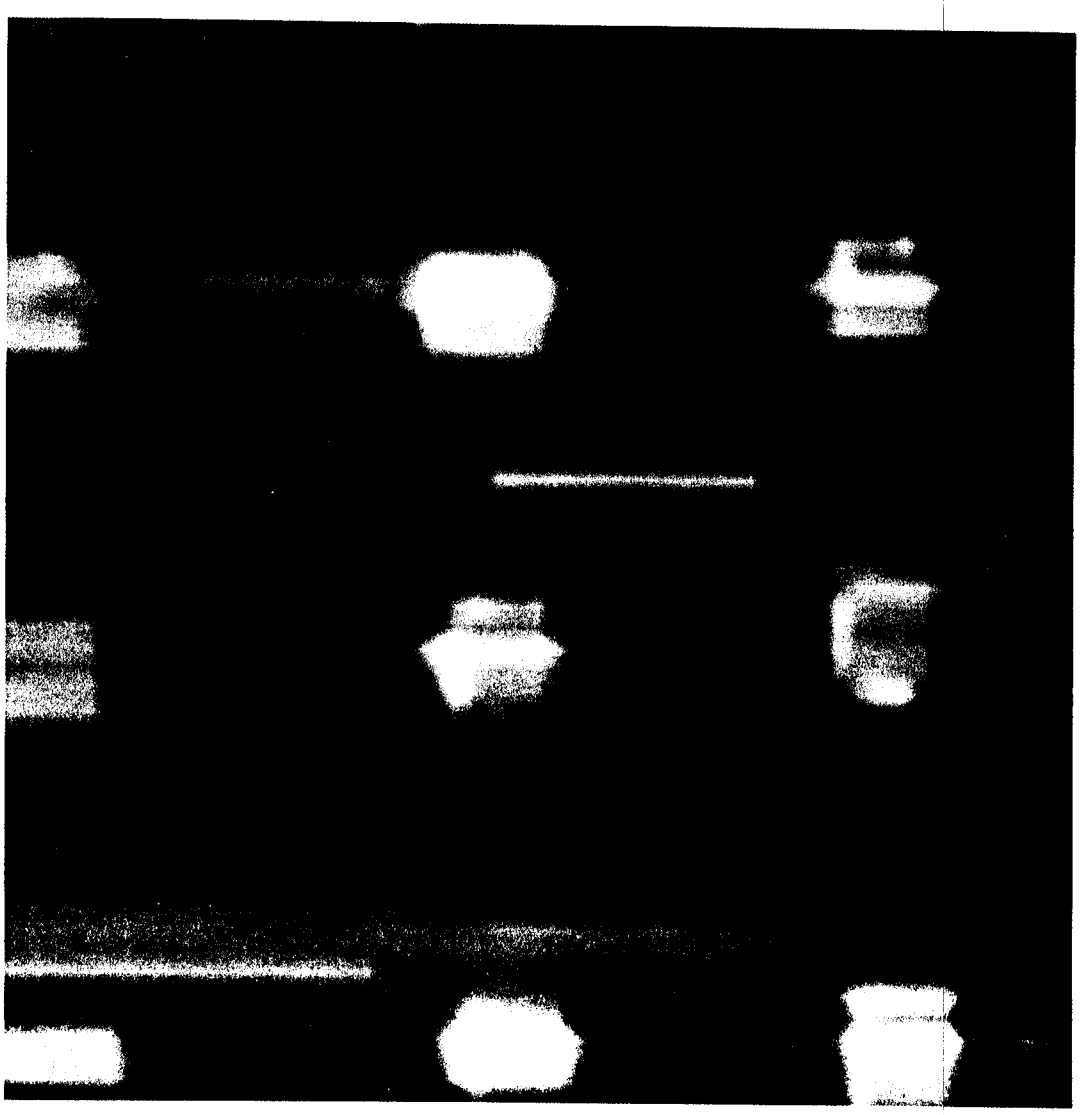

FIG. 2. A 6 μm $\times$ 6 μm topographic image of nine Permalloy bits (nominally 0.5 μm square) on a Si substrate. The grey scale spans approximately 90 nm in height, and no correction has been made for nonlinearities on the piezo displacement. An emission current was maintained at 10 nA with a tip bias of -32 V, resulting in a tip–sample distance of $\sim$90 nm.

multiply scattered primary electrons for the emitter voltages shown in Fig. 3. Slight edge enhancement, typical of secondary images, is also evident in some of the profiles as well as in Fig. 5(b). This occurs predominantly along the right edges in the figures—which is actually the top during measurements and hence closest to the extraction optics.

Model fits to the bit profiles (shown as dashed lines in Fig. 3) were used to determine the resolution of this particular probe tip for different values of the applied bias potential. The model consists of the convolution of a Gaussian function with a square well of variable width and height. Bit widths determined by least-squares fitting ranged from 0.60 to 0.67 μm, slightly larger than expected from the nominal dimension of 0.5 μm, and well beyond the distortions found due to nonlinearities in the piezo displacement. The Gaussian full width at half-maximum is plotted as a function of tip–sample separation in Fig. 4 for each of the model fits in the preceding figure. Also shown is the relation between tip bias and distance for this emitter tip. The distance is determined by monitoring the change in Z-piezo displacement from -8 V tip bias (nearly in the tunneling regime) to the bias voltage required for the measurement. For this tip, the resolution limit appears to be near 50 nm, which includes the expected edge width of <30 nm. We emphasize that the resolution is affected by the topography as well as the tip shape. In particular, near the relatively high edge of the Permalloy bit, fields at the tip may be significantly altered, causing a redistribution of the emission current density that will degrade the resolution. On a poorly cleaned Co sample using a different emitter tip we have resolved features of about 15 nm width, the limit in this case most likely being the size of the features themselves. McCord and Pease[20] have calculated the resolution expected from scanned field emission tips for lithographic applications, however, their parameters are

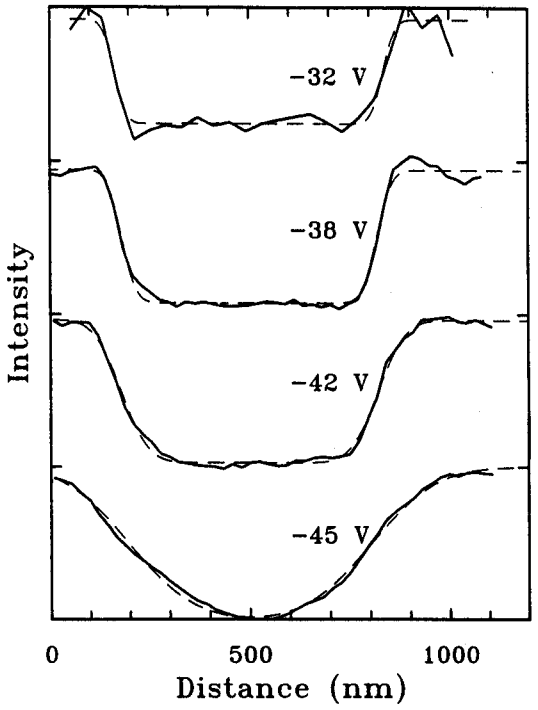

FIG. 3. Solid lines: Profiles of collected electron intensity obtained from scans across the central bit of Fig. 2 for the indicated emitter voltages. Dashed lines: Model fits to the data (see the text). The average minimum and maximum count rates for the − 32 V emitter are 3 and 4 kHz, respectively. The corresponding numbers for − 38 V are 21 and 32 kHz, 31 and 52 kHz for the − 42 V emitter, and for the − 45 V tip 42 and 78 kHz. The emission current was 10 nA in all cases. The curves are offset vertically from each other for clarity.

sufficiently different as to preclude direct comparison to the present data.

Figure 5 compares topographic, electron intensity, and

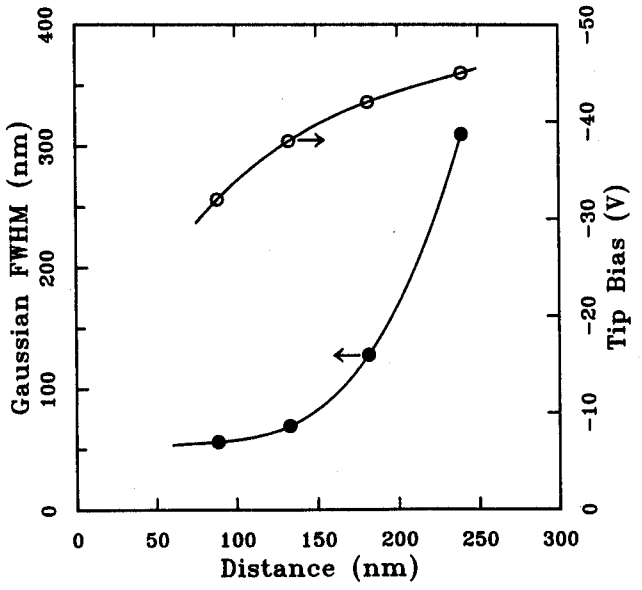

FIG. 4. Summary of spatial resolution (determined by the Gaussian component of the fits in Fig 3) vs tip–sample distance (filled circles), as well as tip bias vs distance (open circles) for a particular field emission tip. These values depend upon the quality of the tip, and in this case are an upper limit to the resolution due to an unknown contribution from the edge width of the Permalloy bit.

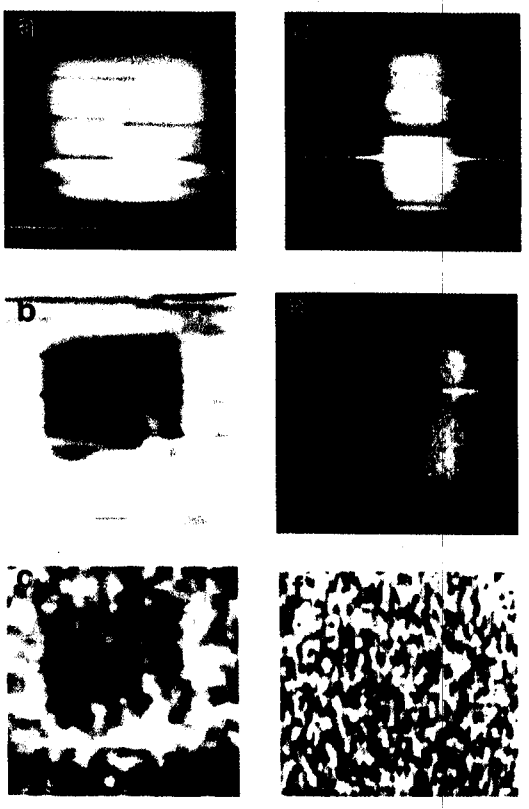

FIG. 5. (a)–(c) Topographic, electron intensity, and M_x magnetization images of the central bit in Fig. 2, simultaneously acquired using an emitter tip prepared by the sputtering technique described in the text. Tip bias − 38 V, 10 nA emission, 1.12 μm × 1.12 μm. (d)–(f). Corresponding images of a 0.5 μm × 1.5 μm bit using an emitter tip prepared by annealing only. Tip bias − 97 V, 10 nA emission current, 2.5 μm × 2.5 μm. The mean height of the bits is 50 nm and the tip–sample separation is approximately 130 nm in both cases. Each magnetization image has been filtered with a two-pole Butterworth low-pass filter of range 100 nm. The right side of these images is actually the top during data acquisition.

M_x magnetization images from two different Permalloy bits, using a low voltage emitter tip prepared by sputtering and a tip treated only by heating to remove contamination. Note that the tip–sample separation is about 130 nm in each case, thus the tip that operates at low voltage must be sharper than the high voltage emitter. The dimensions of the two bits are not the same: 0.5 μm × 0.5 μm for the − 38 V images [Figs. 5(a)–5(c)] and 0.5 μm × 1.5 μm for the − 97 V images [Figs. 5(d)–5(f)]. Slight damage to the bit shown in Figs. 5(a)–5(c) may have been incurred on the first scan of the area. For each bit the three different images (as well as that for M_z) are acquired simultaneously and thus are not subject to any relative shifts due to thermal drift or piezocreep. Here M_z images are featureless for both bits, as expected, since the magnetization for these thin films lies in the plane of the film. The initial plan for these experiments was to magnetize the bits in the positive X direction, image the magnetization, then reverse the magnetization to see if the magnetic contrast reverses. This course has not been completed as yet; however, the preliminary data of Fig. 5 show several interesting features.

First, the topographs of Figs. 5(a) and 5(d) are substan-

tially the same, with somewhat lower resolution for the −97 V emitter. Some degradation of the topographic resolution is expected at higher voltages; McCord and Pease[15] find that the minimum beam radius increases with voltage for their optimum tip. By contrast, the intensity images shown in Figs. 5(b) and 5(e) are strikingly different. For the low voltage emitter tip, the bit appears as a well defined decrease in collected electron intensity, as discussed previously, whereas the image acquired using the high voltage emitter shows an increase in electron yield over the magnetic bit, and further exhibits a distinct left–right asymmetry not present in the corresponding topograph. A profile across the center of Fig. 5(e) shows a large peak approximately 0.40 μm FWHM (slightly larger than the edge width in the topograph) and a smaller peak to its left. The higher yield peak is coincident with the edge of the Permalloy bit closest to the electron extraction optics, while the subsidiary maximum lies next to the opposite edge, shifted slightly toward the extraction column. To understand the origin of these features, one must realize that the tip voltage of −97 V is beyond the bandpass of the electron optics, therefore the intensity image of Fig. 5(e) is undoubtedly due to low energy secondaries. It appears likely that the image is dominated by strong but poorly resolved enhancement of the secondary yield at the edges of the bit. This edge enhancement is a geometrical effect well known in SEM work;[21] it creates a strong asymmetry here simply because of the highly asymmetric collection geometry.

Finally, the M_x magnetization images of Figs. 5(c) and 5(f) are distinctly different in that the low voltage emitter shows some signal due to the presence of the magnetic bit, while none is detected for the high voltage tip. Note that the counting times were 1975 sec/μm^2 for Fig. 5(c), and only 80 sec/μm^2 for Fig. 5(f), however, smaller images with a factor 20 greater counting time still showed no magnetization signal for the −97 V tip. Considering that Fig. 5(e) is dominated by edge effects and poor resolution, the lack of attendant magnetization signal may not be too surprising. The polarization of emitted secondary electrons is also more likely to be randomized by multiple reflections from the sample surface for this high tip bias.[2,15] The appearance of a weak signal in Fig. 5(c) is another matter, however. At present, we cannot determine with certainty that this signal is really due to the magnetization of the Permalloy bit. An alternative explanation would be that a topography-induced asymmetry is present in the angular distribution of collected electrons, mimicking the spin-orbit scattering asymmetry that is the basis for detection in the spin-analyzer. However, we are encouraged by the fact that no topographic features are detected in either M_z or the magnetization image of Fig. 5(f), where the corresponding intensity map, Fig. 5(e), shows dramatic effects due to underlying topography.

IV. SUMMARY

A preliminary report has been presented concerning work in progress to determine the feasibility of directly imaging the magnetization of ferromagnetic samples under the STM. The UHV system employed was designed to be flexible enough to test several different proposals; we have begun with the scanning field emission analog of the successful SEMPA technique. Although atomic resolution will not be achieved with this technique, it has advantages for studying ferromagnetic samples—thin films in particular—in that a nonmagnetic probe is used and the full vector magnetization may be detected. The ability to "zoom" between atomic resolution STM topographs and magnetization images on a somewhat coarser scale should also provide a rather direct correlation between morphology or growth characteristics and the accompanying magnetic structure. Experience gained using scanned field emitters for this purpose is also expected to apply to related techniques such as scanning field emission Auger microscopy.

The results are as yet inconclusive. A weak signal has been observed corresponding to one of the in-plane components of magnetization. However, topographic feedthrough into the magnetization image has not been eliminated as a possible source of the contrast. While there are signs that the topography has little effect on the magnetization signal, more conclusive experiments must be performed to establish this with confidence.

ACKNOWLEDGMENTS

We would like to thank H.-W. Fink for an extended discussion of tip preparation, as well as A. J. Melmed for useful advice. Electron optics calculations and suggestions from M. R. Scheinfein were also very useful, as was the technical support of the NIST Electron Physics Group. This work was supported in part by the Office of Naval Research.

[1] L. M. Falicov, D. T. Pierce, S. D. Bader, R. Gronsky, K. B. Hathaway, H. J. Hopster, D. N. Lambeth, S. S. P. Parkin, G. A. Prinz, M. B. Salamon, I. K. Schuller, and R. H. Victora, J. Mater. Res. **5**, 1299 (1990).
[2] D. T. Pierce, Phys. Scr. **38**, 291 (1988).
[3] D. T. Pierce, M. R. Scheinfein, J. Unguris, and R. J. Celotta, Mater. Res. Soc. Symp. Proc. **151**, 49 (1989).
[4] H.-W. Fink, IBM J. Res. Dev. **30**, 460 (1986).
[5] H.-W. Fink, Phys. Scr. **38**, 260 (1988).
[6] M. R. Scheinfein, J. Unguris, M. H. Kelley, D. T. Pierce, and R. J. Celotta, Rev. Sci. Instrum. **61**, 2501 (1990).
[7] R. Young, J. Ward, and F. Scire, Rev Sci. Instrum. **43**, 999 (1972).
[8] J. Unguris, D. T. Pierce, and R. J. Celotta, Rev. Sci. Instrum. **57**, 1314 (1986).
[9] M. R. Scheinfein, D. T. Pierce, J. Unguris, J. J. McClelland, R. J. Celotta, and M. H. Kelley, Rev. Sci. Instrum. **60**, 1 (1989).
[10] J. W. Lyding, S. Skala, J. S. Hubacek, R. Brockenbrough, and G. Gammie, J. Microsc. **152**, 371 (1988).
[11] A. J. Melmed and J. J. Carroll, J. Vac. Sci. Technol. A **2**, 1388 (1984).
[12] Burleigh Instruments, Inc. This item of commercial equipment is identified in this paper to specify experimental procedures. In no case does this identification imply recommendation or endorsement by the National Institute of Standards and Technology, nor does it imply that the equipment identified is necessarily the best available for the purpose.
[13] E. W. Müller and T. T. Tsong, *Field Ion Microscopy, Principles and Application* (Elsevier, New York, 1969).
[14] R. Allenspach and A. Bischof, Appl. Phys. Lett. **54**, 587 (1989).
[15] M. A. McCord and R. F. W. Pease, Surf. Sci. **181**, 278 (1987).
[16] A. P. Janssen and J. P. Jones, J. Phys. D **4**, 118 (1971).
[17] G. A. Mulhollan, X. Zhang, F. B. Dunning, and G. K. Walters, Phys. Rev. B **39**, 8715 (1989).
[18] We are indebted to J. F. Smyth of UC—San Diego for the loan of the sample.
[19] J. Unguris (private communication).
[20] M. A. McCord and R. F. W. Pease, J. Vac. Sci. Technol. B **3**, 198 (1985).
[21] H. Seiler, J. Appl. Phys. **54**, R1 (1983).